Deep time evidence for climate sensitivity increase with warming

Climate Sensitivity Rise With Warming

Shaffer, Gary; Huber, Matthew; Rondanelli, Roberto; Pedersen, Jens Olaf Pepke

Published in:
Geophysical Research Letters

Link to article, DOI:
10.1002/2016GL069243

Publication date:
2016

Document Version
Publisher's PDF, also known as Version of record

AGU PUBLICATIONS

Geophysical Research Letters

RESEARCH LETTER
10.1002/2016GL069243

Key Points:
- Data-model evidence for climate sensitivity increase with global warming
- Climate sensitivity greater for the warm late Paleocene than for cooler recent times
- Constrained estimates for atmospheric CO_2 content before and during the PETM

Supporting Information:
- Supporting Information S1

Correspondence to:
G. Shaffer,
gary.shaffer.chile@gmail.com

Citation:
Shaffer, G., M. Huber, R. Rondanelli, and J. O. Pepke Pedersen (2016), Deep time evidence for climate sensitivity increase with warming, *Geophys. Res. Lett.*, *43*, 6538–6545, doi:10.1002/2016GL069243.

Received 21 APR 2016
Accepted 8 JUN 2016
Accepted article online 23 JUN 2016
Published online 29 JUN 2016

Deep time evidence for climate sensitivity increase with warming

Gary Shaffer[1,2], Matthew Huber[3,4], Roberto Rondanelli[5,6], and Jens Olaf Pepke Pedersen[7]

[1]GAIA-Antarctica, Universidad de Magallanes, Punta Arenas, Chile, [2]Niels Bohr Institute, University of Copenhagen, Copenhagen, Denmark, [3]Earth, Atmospheric and Planetary Sciences, Purdue University, West Lafayette, Indiana, USA, [4]Institute for the Study of Earth, Oceans, and Space, University of New Hampshire, Durham, New Hampshire, USA, [5]Department of Geophysics, University of Chile, Santiago, Chile, [6]Center for Climate and Resilience Research, University of Chile, Santiago, Chile, [7]National Space Institute, Technical University of Denmark, Kongens Lyngby, Denmark

Abstract Future global warming from anthropogenic greenhouse gas emissions will depend on climate feedbacks, the effect of which is expressed by climate sensitivity, the warming for a doubling of atmospheric CO_2 content. It is not clear how feedbacks, sensitivity, and temperature will evolve in our warming world, but past warming events may provide insight. Here we employ paleoreconstructions and new climate-carbon model simulations in a novel framework to explore a wide scenario range for the Paleocene-Eocene Thermal Maximum (PETM) carbon release and global warming event 55.8 Ma ago, a possible future warming analogue. We obtain constrained estimates of CO_2 and climate sensitivity before and during the PETM and of the PETM carbon input amount and nature. Sensitivity increased from 3.3–5.6 to 3.7–6.5 K (Kelvin) into the PETM. When taken together with Last Glacial Maximum and modern estimates, this result indicates climate sensitivity increase with global warming.

1. Introduction

The quantification of climate sensitivity (CS) is arguably the major challenge of climate science. Present CS estimates are 1.5–4.5 K, a range mostly expressing variations in climate system feedbacks among coupled climate models, whereby cloud feedbacks are particularly uncertain [*Flato et al.*, 2013; *Bony et al.*, 2015; *Sherwood et al.*, 2014]. Furthermore, climate system feedbacks may be climate dependent [*Caballero and Huber*, 2013]. How will such feedbacks and therewith climate sensitivity respond to ongoing global warming from anthropogenic greenhouse gas emissions?

There have been several recent attempts to constrain CS using paleoreconstructions for different periods in the past, but the most robust of these from a data availability perspective are for cold glacial conditions [e.g., *Schmittner et al.*, 2011]. Across the Paleocene-Eocene Thermal Maximum (PETM), the Earth experienced rapid warming of about 5°C from a mean global temperature already about 10°C warmer than present day [*Dunkley Jones et al.*, 2013; *Lunt et al.*, 2012]. This global warming event was driven by carbon emissions to the atmosphere leading to increased greenhouse gas forcing [*Pagani et al.*, 2006; *Zachos et al.*, 2008]. The PETM has been the focus of much study during the past 20 years, in part motivated by its potential relevance to ongoing warming [e.g., *Dickens et al.*, 1995; *Zachos et al.*, 2008]. But uncertainty remains with regard to the source and amount of the PETM carbon input and the climate response to this input [*Pagani et al.*, 2006; *Zachos et al.*, 2005; *Zeebe et al.*, 2009]. Climate-carbon modeling studies with model-dependent CS values and a priori ocean carbon inventory choices and constrained by specific paleoreconstructions have yielded different and even mutually exclusive results [*Panchuk et al.*, 2008; *Zeebe et al.*, 2009; *Cui et al.*, 2011; *Meissner et al.*, 2014]. Here we introduce a new framework for synthesizing the large and diverse body of paleoreconstructions from the PETM and adjacent Eocene times and carry out comprehensive climate-carbon simulations using a relatively simple but well-tested and flexible Earth System Model [*Shaffer et al.*, 2008; *Eby et al.*, 2013]. Our results provide constrained estimates for CS dependence on climate in a warming world and shed new light upon the PETM itself.

2. Climate Sensitivity and Atmospheric CO_2

PETM ocean surface warming was about 5°C with little polar amplification [*Dunkley Jones et al.*, 2013]. Model results indicate that mean atmospheric warming probably was slightly larger [*Lunt et al.*, 2012].

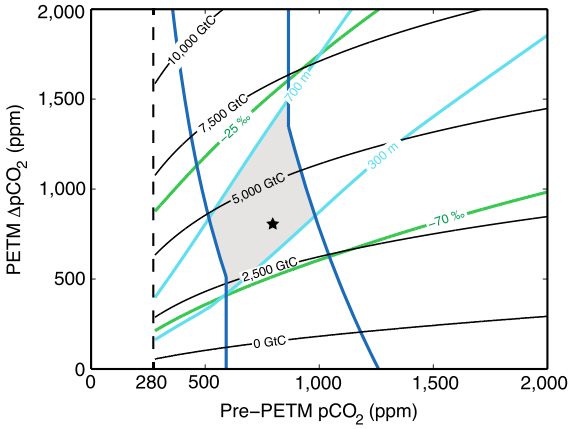

Figure 1. Mineralogical, carbon chemistry, and carbon isotope constraints on possible ranges of pre-PETM pCO_2 and PETM ΔpCO_2. Plotted are (1) lower and upper bounds on pre-PETM pCO_2 from the existence of the mineral nahcolite (dark blue lines; see text), (2) carbon input over a 10,000 year timescale needed to force a PETM ΔpCO_2 from a given pre-PETM pCO_2 level for a 5°C PETM mean atmospheric temperature increase (black lines), (3) isolines for 300 and 700 m shoaling of low-middle latitude CCD depth for the carbon inputs (light blue lines), and (4) isolines of −25 and −70‰ for $\delta^{13}C$ of the carbon inputs producing a −3.5‰ change in the total carbon inventory (green lines). The area defined by the constraints is shaded. The vertical dashed line marks the PI pCO_2 level (280 ppm), and the star marks a possible PETM scenario (see text).

A small fraction of this rise might be ascribed to higher concentrations of minor greenhouse gases; however, most of the warming must be explained by greater pCO_2 from a large carbon input to the ocean-atmosphere system, as evidenced by the PETM carbon isotope excursion (CIE) [*Dunkley Jones et al.*, 2013; *Zachos et al.*, 2008; *Pagani et al.*, 2006; *McInerney and Wing*, 2011]. Much of this input may have been as methane that is oxidized to CO_2 over decadal timescales whereby enhanced pCO_2 radiative forcing dwarfs that from enhanced methane for the input times considered here (Text S1 in the supporting information). We can relate PETM pCO_2 excursion ($\Delta pCO_{2(\mathrm{PETM})}$), pre-PETM pCO_2 ($pCO_{2(\mathrm{pre\text{-}PETM})}$), and PETM climate sensitivity (CS_{PETM}) by

$$CS_{\mathrm{PETM}} = \Delta T_{\mathrm{PETM}} \ln(2) / \ln\left\{\left(pCO_{2(\mathrm{pre\text{-}PETM})} + \Delta pCO_{2(\mathrm{PETM})}\right) / pCO_{2(\mathrm{pre\text{-}PETM})}\right\} \quad (1)$$

where CS refers to temperature increase after ocean heat equilibration and ΔT_{PETM} is the mean atmospheric temperature (MAT) rise over the PETM from pCO_2 increase, taken here to be 5°C. An analogous expression for pre-PETM climate sensitivity ($CS_{\mathrm{pre\text{-}PETM}}$) is

$$CS_{\mathrm{pre\text{-}PETM}} = \Delta T_{\mathrm{pre\text{-}PETM}} \ln(2) / \ln\left(pCO_{2(\mathrm{pre\text{-}PETM})} / pCO_{2(\mathrm{PI})}\right) \quad (2)$$

where $\Delta T_{\mathrm{pre\text{-}PETM}}$ is the part of the MAT difference between pre-PETM and preindustrial (PI) times due to higher pCO_2 and $pCO_{2(\mathrm{PI})}$ is 280 ppm. Pre-PETM conditions can be estimated by comparing late Paleocene deep ocean and surface temperature records and considered within the context of subsequent, nonhyperthermal, early Eocene records for which more data exist. From these, we can glean that pre-PETM MAT was ~10°C warmer than PI [*Huber and Caballero*, 2011; *Lunt et al.*, 2012; *Zachos et al.*, 2008]. Much of this extra warmth may derive from albedo reduction from much reduced high-latitude ice and snow, complemented by low-latitude, albedo reductions from reduced subtropical landmass [*Herold et al.*, 2014] (Figure S1) and increased land vegetation cover [*Huber and Caballero*, 2011]. Aerosol decrease and higher minor greenhouse gas concentrations may have each enhanced warming by ~1°C [*Lunt et al.*, 2012]. From model results that include these factors [*Huber and Caballero*, 2011; *Lunt et al.*, 2012], we estimate that they may account for about 4°C of the warming leaving about 6°C to be explained by greater atmospheric pCO_2. Thus, we take $\Delta T_{\mathrm{pre\text{-}PETM}}$ to be 6°C.

From equations (1) and (2) with the above choices for MAT increases due to pCO_2 we can deduce possible ranges for pre-PETM and PETM CS from estimates of pre-PETM pCO_2 and the PETM pCO_2 excursion. Here we use proxy data and carbon cycle modeling to obtain such estimates and plot the results in a space defined by pre-PETM pCO_2 and the PETM pCO_2 excursion (Figure 1). In this way we constrain a possible area in this pCO_2 space and thereby also possible ranges for pre-PETM and PETM CS.

3. Mineralogical, Carbon Cycle, and Isotope Constraints

3.1. Nahcolite

One constraint derives from the existence of the mineral nahcolite in the Green River Formation, USA, from the Early Eocene Climatic Optimum (EECO) about 51 Ma ago and from stability fields of sodium carbonate

forms (nahcolite, trona, and natron) as functions of temperature and pCO_2 [*Lowenstein and Demicco*, 2006; *Jagniecki et al*., 2015]. While the original work derived a lower bound on EECO pCO_2 of about 1125 ppm from the triple point where these forms are at equilibrium (in the presence of halite), the recent analysis based on new experimental data puts this point at 680 ppm and a temperature of 19.5°C. Furthermore, homogenization temperatures for fluid inclusions in halite in this formation were found to be 21 to 28°C. Together with the new stability fields, this translates to minimum and maximum estimates for EECO pCO_2 of 760 and 1260 ppm [*Jagniecki et al*., 2015]. Below we show how these results can constrain pre-PETM pCO_2 and the PETM pCO_2 excursion.

Pre-PETM temperatures were about 2°C cooler than during the EECO [*Zachos et al*., 2008], likely due to less greenhouse gas forcing given similarity between pre-PETM and EECO boundary conditions. With this and the results above, we can estimate bounds on EECO CS using

$$CS_{EECO} = \Delta T_{EECO} \ln(2) / \ln\left(pCO_{2(\text{pre-PETM})} / pCO_{2(EECO)}\right) \quad (3)$$

with $\Delta T_{EECO} = -2$°C. Since the EECO was warmer than pre-PETM but cooler than the PETM, it is reasonable to assume that CS_{EECO} lies between CS for these periods. If $CS_{PETM} > CS_{\text{pre-PETM}}$, this and the results above imply a lower bound on pre-PETM pCO_2 when $CS_{EECO} = CS_{\text{pre-PETM}}$ and $pCO_{2(EECO)} = 760$ ppm and an upper bound relationship between pre-PETM pCO_2 and PETM ΔpCO_2 when $CS_{EECO} = CS_{PETM}$ and $pCO_{2(EECO)} = 1260$ ppm. If $CS_{\text{pre-PETM}} > CS_{PETM}$, this implies a lower bound relationship between pre-PETM pCO_2 and PETM ΔpCO_2 excursion when $CS_{EECO} = CS_{PETM}$ and $pCO_{2(EECO)} = 760$ ppm and an upper bound on pre-PETM pCO_2 when $CS_{EECO} = CS_{\text{pre-PETM}}$ and $pCO_{2(EECO)} = 1260$ ppm. These conditions and equations (1)–(3) yield the two dark blue lines in Figure 1; acceptable values for pre-PETM pCO_2 and PETM ΔpCO_2 lie between the lines.

3.2. Pre-PETM Conditions

Observations of carbon isotopes and carbonate compensation depths (CCD) together with ocean carbonate chemistry and carbon cycle modeling provide further constraints. Previous PETM carbon cycle models have used a priori choices for pre-PETM pCO_2 (with associated ocean carbon inventory) and constant ocean phosphate inventories [*Panchuk et al*., 2008; *Zeebe et al*., 2009; *Cui et al*., 2011; *Meissner et al*., 2014]. We take a more general approach by considering the wide range of possible pre-PETM pCO_2 values from proxy reconstructions [*Zachos et al*., 2008; *Beerling and Royer*, 2011] and climate-dependent weathering including phosphate input to the ocean. For given lithosphere carbon emissions and weathering intensities, steady state conditions are established on million year timescales. For such conditions in the Danish Center for Earth System Science (DCESS) model used here [*Shaffer et al*., 2008], carbon and phosphate sources from lithosphere outgassing and/or weathering balance carbon and phosphate sinks in ocean sediment burial of organic matter and/or $CaCO_3$ (Text S1). Given the slowly varying climate prior to the PETM [*Zachos et al*., 2008], we seek steady state solutions as initial conditions for PETM simulations.

Model radiative forcing was adapted to early Eocene conditions for solar forcing, albedo, high-latitude radiative forcing, and greenhouse gas concentrations to achieve in long model integrations mean atmospheric and deep ocean temperatures of 25°C and 10°C, respectively [*Huber and Caballero*, 2011; *Lunt et al*., 2012; *Zachos et al*., 2008] (Text S1). These temperatures were prescribed (bypassing the climate part of the model), ocean chemistry was adjusted to late Paleocene values, and biogeochemical steady states were sought for the full range of possible pre-PETM pCO_2 (Text S1 and Table S1). One difference between pre-PETM and PI simulations is the more diffuse, pre-PETM lysocline (Figure S2). A reconstruction of the pre-PETM lysocline shows a rather diffuse lysocline in the tropical Pacific Ocean [*Panchuk et al*., 2008]. An Indian Ocean reconstruction [*Panchuk et al*., 2008] appears sharper, but this may be an artifact of juxtaposition of subtropical sediment cores from ~5 km paleodepths with high-latitude cores at shallower paleodepths, in particular from well-documented Deep Sea Drilling Project site 259 [*Zeebe et al*., 2009; *Hancock et al*., 2009] (pre-PETM latitude and water depth of about 55°S and 4000 m). Another pre-PETM/PI simulation difference is high $CaCO_3$ accumulation in deep, high-latitude pre-PETM sediments (Figure S2h). This stems from greater model biogenic $CaCO_3$ production from warmer pre-PETM high-latitude surface layer temperatures (see parameterization in Text S1). Pre-PETM $CaCO_3$ content ($CaCO_3$ wt %) at 4000 m depth of about 50% are found in both the high-latitude model zone and in the data from site 259, the one high-latitude core with deep paleodepth available to test this.

Model steady state relationships between pre-PETM pCO_2 and carbon inventories for the standard pre-PETM MAT are given in Table S1 and plotted in Figure S3. For an ocean carbon inventory like PI but with late Paleocene conditions, atmospheric pCO_2 values are about 4 times greater than PI. This enhancement is due mainly to much higher ocean calcium content in the pre-PETM ocean and lower CO_2 solubility at higher temperatures. These properties and coupling to calcite saturation elevate ocean [CO_2] and depress ocean [CO_3^{2-}]. Model land biosphere inventories are somewhat higher for higher pre-PETM pCO_2 from carbon fertilization (Figure S3).

3.3. Exploratory Simulations

The above steady states provide initial conditions for a series of 20,000 year simulations of the PETM initial phase for prescribed carbon inputs of different sizes but common time evolutions and for a common prescribed PETM MAT evolution with 5°C maximum warming (Text S1). This procedure again bypasses the climate part of the model to concentrate on carbon cycle response. PETM ΔpCO_2 values are given in Table S2 and contoured in pCO_2 space as carbon inputs in Figure 1. There is a significant pCO_2 increase from the warming alone (0 carbon input isoline in Figure 1) due to ocean outgassing from less CO_2 solubility and soil outgassing from more bacterial activity. Recalculations of PETM ΔpCO_2 values using constant, pre-PETM ratios carbonate to organic carbon production (rain ratios) show only modest changes (Table S2).

Carbon inputs to the atmosphere-ocean system lead to ocean acidification and $CaCO_3$ dissolution in the ocean sediment as well as decreased model biogenic $CaCO_3$ production (Text S1). These effects force shoaling of the CCD (here the depth of 10% $CaCO_3$ wt %). On the other hand, warming promotes increased biogenic $CaCO_3$ production from enhanced weathering that raises ocean phosphate concentrations and thereby new production as well as from enhanced rain ratios, an effect shown above to reproduce observed high $CaCO_3$ wt % in the deep, high-latitude, pre-PETM ocean. Increased biogenic $CaCO_3$ production forces CCD deepening. These opposing effects are reflected in model maximum, low-middle latitude CCD excursions for the PETM (Table S3 and Figure S4). For the PETM warming alone (0 carbon input) and our standard rain ratio expression (equation (S6)) the low-middle latitude CCD deepens by about 400 m. A recalculation using constant, pre-PETM rain ratios shows somewhat less shoaling (Table S3).

Observed low-middle latitude CCD shoaling across the PETM ranged from a few hundred meters in the Pacific Ocean to more than 2000 m in the South Atlantic Ocean [*Panchuk et al*., 2008; *Zeebe et al*., 2009]. Observations from the Indian Ocean indicate modest shoaling as in the Pacific [*Zeebe et al*., 2009]. In the late Paleocene/early Eocene, the Pacific Ocean was larger and the South Atlantic Ocean considerably smaller than now, accounting then for 57% and 7% of total, low-middle latitude ocean area, respectively (Table S4). If a South Atlantic CCD shoaling of 2000 m is taken to apply there only and a 200 m shoaling is assumed for the rest of the ocean, with basin size weighting we obtain a lower bound estimate on PETM CCD shoaling of 329 m that we round down to 300 m. If the South Atlantic shoaling is taken to apply to the whole Atlantic and a 400 m shoaling is assumed for the rest of the ocean, with this weighting we obtain an upper bound shoaling estimate of 673 m that we round up to 700 m. Thus, we adopt 300–700 m as our observation-based range for global mean, maximum low-middle latitude, PETM CCD shoaling.

For a pre-PETM carbon inventory similar to present day, this 300–700 m shoaling range is reproduced in the model for a carbon input of 2920–6530 Gt C (Figure S4; pre-PETM $pCO_2 = 800$). Without the warming feedbacks, i.e., with constant weathering, pre-PETM new production, and rain ratios, a much lower input of 1010–3150 Gt C forces such shoaling. This is an input range similar to that found in *Zeebe et al*. [2009] who did not consider warming feedbacks and thereby likely underestimated the PETM carbon input consistent with observed CCD shoaling. There are large uncertainties in modeling weathering and biosphere response to warming, but such nutrient and carbon cycle feedbacks were surely important for the workings of the PETM global warming event and should be addressed in PETM simulations.

Observed PETM CIEs vary from -2.5 ± 1.0‰ for benthic forams, -2.7 ± 1.0‰ for planktonic forams, -2.7 ± 1.1‰ for marine bulk carbonate, -4.1 ± 2.2‰ for marine organic matter, and -4.7 ± 1.5‰ for terrestrial records [*McInerney and Wing*, 2011]. These results are consistent with increased carbon isotope discrimination during photosynthesis for more dissolved CO_2 in the ocean surface layer, as implemented here (Text S1). PETM terrestrial records probably also reflect more carbon isotope discrimination during photosynthesis, for example, from increased humidity or pCO_2 [*Bowen et al*., 2004; *Schubert and Jahren*, 2013]. On the other hand, marine

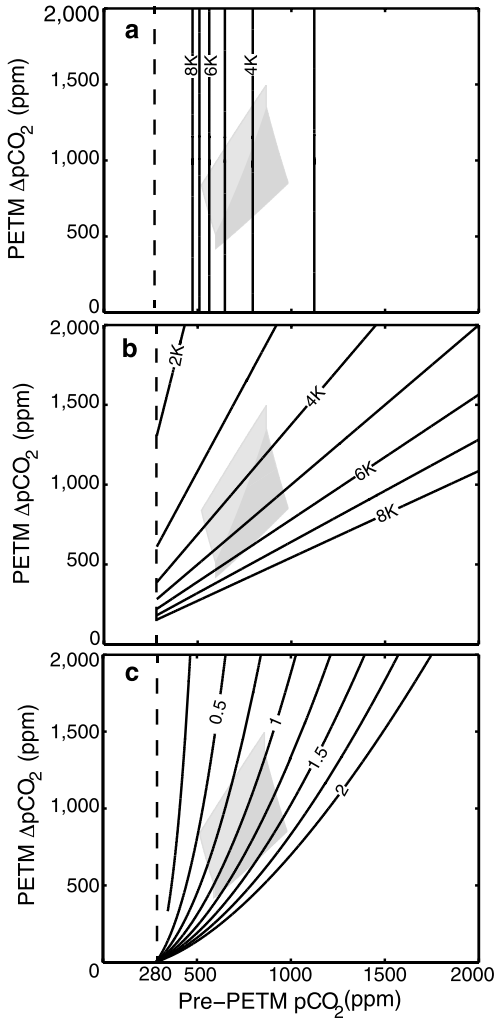

Figure 2. Climate sensitivity (CS) ranges consistent with mineralogical, carbon chemistry, and carbon isotope constraints. (a) Pre-PETM CS, (b) PETM CS, and (c) (PETM CS)/(Pre-PETM CS). CS values were calculated using equations (1) and (2). Acceptable values are in the (shaded) constrained area in pCO_2 space from Figure 1. Darker shading marks values for which PETM CS ≥ Pre-PETM CS. The vertical dashed line marks the PI pCO_2 level (280 ppm).

carbonates may experience increased dissolution across the PETM and may therefore underestimate the CIE at some sites. Therefore, a "true" CIE from external carbon input is probably somewhat larger than the marine carbonate records and we choose a mean ocean-atmosphere-biosphere CIE, CIE^{tot}, of −3.5‰ as our data-based target. With this and the above results we can now calculate the input $\delta^{13}C$ content, $\delta^{13}CI^{tot}$, for given model carbon input and initial conditions (Text S1). The results are contoured in pCO_2 space in Figure S5. Possible PETM carbon input sources include organic carbon (about −25‰ in early Eocene times) [*Falkowski et al.*, 2005], thermogenic methane (−35 to −45‰), and methane hydrate (−60 to −70‰). Volcanic carbon (−5 to −7‰) can probably be ruled out as a primary source: the very large volcanic carbon input needed to explain the observed CIE greatly exceeds inputs consistent with observed CCD shoaling. Therefore, we take $\delta^{13}CI^{tot}$ to lie between −25 and −70‰.

4. Atmospheric CO_2, PETM Carbon Input, and Climate Sensitivity

The shaded area in Figure 1 defines the pCO_2 space for which all the above mineralogical, carbon cycling, and isotope constraints are satisfied. Pre-PETM pCO_2 is found to lie between 512 and 982 ppm with pre-PETM total carbon inventories between 30,780 and 40,000 Gt C. The PETM pCO_2 increase lies between 416 and 1500 ppm, corresponding to PETM carbon inputs of 2090 Gt C ($\delta^{13}C = -68.5$‰) to 6890 Gt C ($\delta^{13}C = -26.4$‰). Note that the range of acceptable pre-PETM pCO_2 is associated with pre-PETM total carbon inventories 0.76–0.99 times as large as a modern-day inventory (Figure S3). For lower initial inventories, less carbon input is needed to achieve observed PETM CCD shoaling and carbon isotope excursions (Figures S4 and S5).

With the use of equations (1) and (2), we can now calculate values for pre-PETM and PETM CS falling within the constrained pCO_2 space of Figure 1. These CS results and their ratios are plotted in Figure 2. We find that pre-PETM CS to lie between 3.3 and 6.8 K, while PETM CS lies between 3.4 and 6.5 K. These CS ranges for MATs of about 25 and 30°C, respectively, both extend well above upper estimates for present-day CS of 1.5–4.5 K [*Flato et al.*, 2013] for a MAT of about 14°C, providing strong evidence for CS increase with warming. A further implication is then that as the Earth warms into the PETM, CS will not likely decrease, i.e., $CS_{PETM}/CS_{pre\text{-}PETM} \geq 1$. This is consistent with recent modeling indicating that any CS decrease with further warming may occur only for much warmer MAT (>40°C) [*Popp et al.*,

2016]. The condition $CS_{PETM}/CS_{pre\text{-}PETM} \geq 1$ further constrains pre-PETM CS, PETM CS, and $CS_{PETM}/CS_{pre\text{-}PETM}$ to the ranges 3.3–5.6 K, 3.7–6.5 K, and 1–1.68, respectively (Figure 2), and also puts slightly tighter bounds on our pCO_2 and carbon input estimates. Pre-PETM pCO_2 now lies between 592 and 982 ppm with pre-PETM total carbon inventories between 32,500 and 40,000 Gt C, and the PETM pCO_2 increase lies between 416 and 1348 ppm, corresponding to PETM carbon inputs of 2090 Gt C ($\delta^{13}C = -68.5‰$) to 6210 Gt C ($\delta^{13}C = -28.8‰$). There would be still tighter bounds on the above properties if constrained by an EECO pCO_2 range of 930–1260 ppm, a range consistent with both the above nahcolite constraint and very recent pCO_2 estimates from boron isotope data [*Anagnostou et al*., 2016].

The above results are quite robust to parameter value choices. For example, for a range of 5–7°C for pre-PETM warmth due to higher pCO_2 ($\Delta T_{pre\text{-}PETM}$ in equation (2)), our analysis yields 572–982 ppm for pre-PETM pCO_2, 398–1460 ppm for the PETM pCO_2 increase, 2020 ($\delta^{13}C = -70‰$)–6780 ($\delta^{13}C = -26.6‰$) Gt C for the carbon input, 2.8–6.3 K for pre-PETM CS, and 3.5–6.6 K for PETM CS. If we choose a CIE^{tot} of −4‰ as our data-based target, we find 592–982 ppm for pre-PETM pCO_2, 454–1348 ppm for PETM pCO_2 increase, 2350 ($\delta^{13}C = -70‰$)–6210 ($\delta^{13}C = -32.8‰$) Gt C for the carbon input, 3.3–5.6 K for pre-PETM CS, and 3.7–6.1 K for PETM CS.

The results in Figure 1 permit a rather broad range of PETM carbon input scenarios, but some appear more likely. The highest permissible carbon input of 6210 Gt C ($\delta^{13}C = -28.8‰$) could be explained by an organic carbon injection, but such an input would be about twice the size of our pre-PETM land biosphere (Figure S3) or that in other work [*Beerling*, 2000]. Organic carbon reserves about half the required size have been proposed for pre-PETM permafrost [*DeConto et al*., 2012]. However, proxy-based reconstructions of high-latitude climate for the late Paleocene/early Eocene show mean surface temperatures well in excess of 10°C [*Huber and Caballero*, 2011; *Lunt et al*., 2012; *Kemp et al*., 2014], too warm to allow extensive permafrost at high latitudes even at elevations above 1000 m. Other explanations in terms of organic carbon also fall short or lack support in the paleorecord [*Panchuk et al*., 2008; *Moore and Kurtz*, 2008]. If for these reasons we rule out organic carbon as the sole source of the PETM carbon input, then this input must have involved considerable amounts of methane.

The lowest permissible input of 2020 Gt C ($\delta^{13}C = -70‰$) could be explained by methane hydrate destabilization. However, there is an ongoing debate as to whether this much methane hydrate could exist for warm pre-PETM conditions [*Buffett and Archer*, 2004; *Gu et al*., 2011]. Such a scenario would require very high CS values with a CS increase into the PETM from 5.6°C to 6.5 K. One possible scenario centered within the acceptable pCO_2 space (star in Figure 1) would be thermogenic methane input [*Svensen et al*., 2004] of 3740 Gt C ($\delta^{13}C = -43.7‰$) into a pre-PETM state with 800 ppm pCO_2 and a total carbon inventory of 36,730 Gt C. This would raise pCO_2 at the PETM maximum to 1600 ppm, lead to a maximum, mean low-middle latitude CCD shoaling of 394 m, and be associated with a CS increase into the PETM from 4.0° to 5.0 K. However, other possibilities cannot be excluded like some combination of more modest amounts than considered above of methane hydrate, thermogenic methane, organic matter, and/or direct volcanic carbon input.

5. Discussion and Conclusions

Here we have taken a new approach to the problem of climate change and carbon cycling across the PETM global warming event. We use new climate reconstructions for late Paleocene-early Eocene conditions and for the PETM to set the stage for an analysis of carbon cycling and climate sensitivity. For that analysis, we compare paleoreconstructions with Earth System model simulations that consider a wide range of possible pre-PETM pCO_2 and associated carbon inventories for pre-PETM ocean chemistry and that include climate feedbacks on nutrient and carbon cycling. For applied pre-PETM and PETM warming, we apply joint mineralogical, carbon chemistry, and carbon isotope constraints to estimate possible ranges of pre-PETM and PETM pCO_2 and the size and nature of the PETM carbon input. Finally, we use these results and some consistency considerations to estimate possible ranges for pre-PETM and PETM CS.

Our pre-PETM CS range of 3.3–5.6 K is for a MAT of about 25°C, while the PETM CS range of 3.7–6.5 K is for a MAT of about 30°C. For comparison, the range of present-day CS estimates is 1.5–4.5 K for a MAT of about 14°C whereby about one fourth this CS is due to ice-albedo feedback [*Flato et al*., 2013], not contributing to CS in the warm late Paleocene era. Furthermore, several recent studies yield present-day CS estimates in the

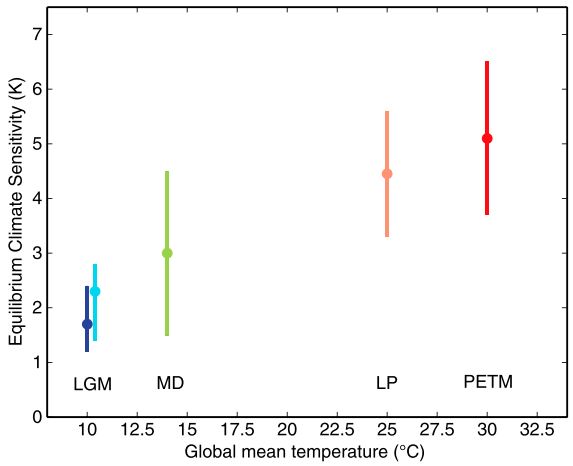

Figure 3. Climate sensitivity range estimates at different global mean atmospheric temperatures. Shown are our pre-PETM/Late Paleocene (LP) and PETM estimates, the modern-day (MD) IPCC estimate [*Flato et al.*, 2013], and several recent Last Glacial Maximum (LGM) estimates (light blue [*Schmittner et al.*, 2011] and dark blue [*Annan and Hargreaves*, 2013]). The large dots represent the central values for the MD, LP, and PETM estimates and the preferred values in the published analyses for the LGM estimates.

lower half of this Intergovernmental Panel on Climate Change (IPCC) range [*Annan*, 2015; *Johansson et al.*, 2015]. Recent estimates of the Last Glacial Maximum CS for a well-defined MAT 3–4°C lower than present also fall at the lower end of present-day estimates [*Schmittner et al.*, 2011; *Annan and Hargreaves*, 2013]. Earlier studies found considerably greater LGM global mean cooling [e.g., *Schneider von Deimling et al.*, 2006] leading to higher CS estimates [e.g., *Köhler et al.*, 2010]. However, the more recent studies cited above use much improved temperature data bases, yielding lower, more accurate CS estimates. Taken together with these LGM and modern-day CS estimates, our results provide strong evidence from observations and model-data comparisons for a CS increase with warming (Figure 3).

In some complex climate system models, CS was found to increase for rising MAT, in particular due to some combination of fast water vapor and cloud feedbacks [*Caballero and Huber*, 2013; *Meraner et al.*, 2013; *Popp et al.*, 2016]. Our results lend some credence to these model findings. The compilation in Figure 3 supports a CS increase with MAT but permits few conclusions on the structure of this increase. One could define a linear increase with MAT based on our results, but these results also allow for an abrupt, nonlinear CS rise for a relatively small warming as was found in the models cited above.

Our findings support the notion that as pCO_2 and global temperatures continue to rise, there may be additional warming as CS may increase despite less ice-albedo feedback as snow and sea ice cover diminish. If warming increases CS, greater CS makes the Earth warm more, amplifying the warming [*Bloch-Johnson et al.*, 2015]. Thus, our results further underline the need to limit ongoing global warming by greatly reducing anthropogenic greenhouse gas emissions as soon as possible.

Acknowledgments
We thank Esteban Fernandez Villanueva for the calculated land distributions. Some of this work was carried out at the Center for Advanced Studies in Desert Zones, La Serena, Chile, and Bornö Institute for Ocean and Climate Studies, Brastad, Sweden. DCESS model code can be downloaded at www.dcess.dk. This work was supported by FONDECYT (Chile) grants 1120040 and 1150913.

References

Anagnostou, E., E. H. John, K. M. Edgar, G. L. Foster, A. Ridgwell, G. N. Inglis, R. D. Pancost, D. J. Lunt, and P. N. Pearson (2016), Changing atmospheric CO_2 concentration was the primary driver of early Cenozoic climate, *Nature*, *533*(7603), 380–384, doi:10.1038/nature17423.

Annan, J. D. (2015), Recent developments in Bayesian estimation of climate sensitivity, *Curr. Clim. Change Rep.*, *1*, 263–267, doi:10.1007/s40641-015-0023-5.

Annan, J. D., and J. C. Hargreaves (2013), A new global reconstruction of temperature changes at the Last Glacial Maximum, *Clim. Past*, *9*, 367–376, doi:10.5194/cp-9-367-2013.

Beerling, D. J. (2000), Increased terrestrial carbon storage across the Palaeocene-Eocene boundary, *Palaeogeogr. Palaeoclim.Palaeoecol.*, *161*(3–4), 395–405, doi:10.1016/S0031-0182(00)00095-X.

Beerling, D. J., and D. L. Royer (2011), Convergent Cenozoic CO_2 history, *Nat. Geosci.*, *4*(7), 418–420, doi:10.1038/ngeo1186.

Bloch-Johnson, J., R. T. Pierrehumbert, and D. S. Abbot (2015), Feedback temperature dependence determines the risk for high warming, *Geophys. Res. Lett.*, *42*, 4973–4980, doi:10.1002/2015GL064240.

Bony, S., et al. (2015), Clouds, circulation and climate sensitivity, *Nat. Geosci.*, *8*(4), 261–268, doi:10.1038/ngeo2398.

Bowen, G. J., D. J. Beerling, P. L. Koch, J. C. Zachos, and T. Quattlebaum (2004), A humid climate state during the Palaeocene/Eocene thermal maximum, *Nature*, *432*(7016), 495–499, doi:10.1038/nature03115.

Buffett, B., and D. E. Archer (2004), Global inventory of methane clathrate: Sensitivity to changes in environmental conditions, *Earth Planet. Sci. Lett.*, *227*(3–4), 185–199, doi:10.1016/j.epsl.2004.09.005.

Caballero, R., and M. Huber (2013), State-dependent climate sensitivity in past warm climates and its implications for future climate projections, *Proc. Natl. Acad. Sci. U.S.A.*, *110*(35), 14,162–14,167, doi:10.1073/pnas.1303365110.

Cui, Y., L. R. Kump, A. J. Ridgwell, A. J. Charles, C. K. Junium, A. F. Diefendorf, K. H. Freeman, N. M. Urban, and I. C. Harding (2011), Slow release of fossil carbon during the Paleocene-Eocene Thermal Maximum, *Nat. Geosci.*, *4*(7), 481–485, doi:10.1038/ngeo1179.

DeConto, R. M., S. Galeotti, M. Pagani, D. Tracy, K. Schaefer, T. Zhang, D. Pollard, and D. J. Beerling (2012), Past extreme warming events linked to massive carbon release from thawing permafrost, *Nature*, *484*(7392), 87–91, doi:10.1038/nature10929.

Dickens, G. R., J. R. O'Neil, D. K. Rea, and R. M. Owen (1995), Dissociation of oceanic methane hydrate as a cause of the carbon-isotope excursion at the end of the Paleocene, *Paleoceanography*, *10*(6), 965–971, doi:10.1029/95PA02087.

Dunkley Jones, T. D., D. J. Lunt, D. N. Schmidt, A. Ridgwell, A. Sluijs, P. J. Valdes, and M. Maslin (2013), Climate model and proxy data constraints on ocean warming across the Paleocene–Eocene Thermal Maximum, *Earth Sci. Rev.*, *125*, 123–145, doi:10.1016/j.earscirev.2013.07.004.

Eby, M., et al. (2013), Historical and idealized climate model experiments: An intercomparison of Earth system models of intermediate complexity, *Clim. Past.*, *9*(3), 1111–1140, doi:10.5194/cp-9-1111-2013.

Falkowski, P. G., M. E. Katz, A. J. Milligan, K. Fennel, B. S. Cramer, M. P. Aubry, R. A. Berner, M. J. Novacek, and W. M. Zapol (2005), The rise of oxygen over the past 205 million years and the evolution of large placental mammals, *Science*, *309*(5744), 2202–2204, doi:10.1126/science.1116047.

Flato, G., et al. (2013), Evaluation of climate models, in *Climate Change 2013: The Physical Science Basis. Contribution of Working Group I to the Fifth Assessment Report of the Intergovernmental Panel on Climate Change*, pp. 741–866, Cambridge Univ. Press, Cambridge.

Gu, G., G. R. Dickens, G. Bhatnagar, F. S. Colwell, G. J. Hirasaki, and W. G. Chapman (2011), Abundant Early Palaeogene marine gas hydrates despite warm deep-ocean temperatures, *Nat. Geosci.*, *4*(12), 848–851, doi:10.1038/ngeo1301.

Hancock, H. J. L., G. R. Dickens, E. Thomas, and K. L. Blake (2009), Reappraisal of early Paleogene CCD curves: Foraminiferal assemblages and stable carbon isotopes across the carbonate facies of Perth Abyssal Plain, *Int. J. Earth Sci.*, *96*(5), 925–946, doi:10.1007/s00531-006-0144-0.

Herold, N., J. Buzan, M. Seton, A. Goldner, J. A. M. Green, R. D. Müller, P. Markwick, and M. Huber (2014), A suite of early Eocene (~55 Ma) climate model boundary conditions, *Geosci. Model Dev.*, *7*(5), 2077–2090, doi:10.5194/gmd-7-2077-2014.

Huber, M., and R. Caballero (2011), The early Eocene equable climate problem revisited, *Clim. Past*, *7*(2), 603–633, doi:10.5194/cp-7-603-2011.

Jagniecki, E. A., T. K. Lowenstein, D. M. Jenkins, and R. V. Demicco (2015), Eocene atmospheric CO_2 from the nahcolite proxy, *Geology*, *43*(12), 1075–1078, doi:10.1130/G36886.1.

Johansson, D. J. A., B. C. O'Neill, C. Tebaldi, and O. Häggström (2015), Equilibrium climate sensitivity in light of observations over the warming hiatus, *Nat. Clim. Change*, *5*, 449–453, doi:10.1038/nclimate2573.

Kemp, D. B., S. A. Robinson, J. A. Crame, J. E. Francis, J. Ineson, R. J. Whittle, V. Bowman, and C. O'Brien (2014), A cool temperate climate on the Antarctic Peninsula through the latest Cretaceous to early Paleogene, *Geology*, *42*(7), 583–586, doi:10.1130/G35512.1.

Köhler, P., R. Bintanja, H. Fischer, F. Joos, R. Knutti, G. Lohmann, and V. Masson-Delmotte (2010), What caused Earth's temperature variations during the last 800,000 years? Data-based evidence on radiative forcing and constraints on climate sensitivity, *Quat. Sci. Rev.*, *29*, 129–145, doi:10.1016/j.quascirev.2009.09.026.

Lowenstein, T. K., and R. V. Demicco (2006), Elevated Eocene atmospheric CO_2 and its subsequent decline, *Science*, *313*(5795), 1928, doi:10.1126/science.1129555.

Lunt, D. J., et al. (2012), A model–data comparison for a multi-model ensemble of early Eocene atmosphere–ocean simulations: EoMIP, *Clim. Past*, *8*(5), 1717–1736, doi:10.5194/cp-8-1717-2012.

McInerney, F. A., and S. L. Wing (2011), The Paleocene-Eocene Thermal Maximum: A perturbation of carbon cycle, climate, and biosphere with implications for the future, *Annu. Rev. Earth Planet. Sci.*, *39*(1), 489–516, doi:10.1146/annurev-earth-040610-133431.

Meissner, K. J., T. J. Bralower, K. Alexander, T. Dunkley Jones, W. Sijp, and M. Ward (2014), The Paleocene-Eocene Thermal Maximum: How much carbon is enough?, *Paleoceanography*, *29*, 946–963, doi:10.1002/2014PA002650.

Meraner, K., T. Mauritsen, and A. Voigt (2013), Robust increase in equilibrium climate sensitivity under global warming, *Geophys. Res. Lett.*, *40*, 5944–5948, doi:10.1002/2013GL058118.

Moore, E. A., and A. C. Kurtz (2008), Black carbon in Paleocene–Eocene boundary sediments: A test of biomass combustion as the PETM trigger, *Palaeogeogr. Palaeoclim.Palaeoecol.*, *267*(1–2), 147–152, doi:10.1016/j.palaeo.2008.06.010.

Pagani, M., K. Caldeira, D. Archer, and J. C. Zachos (2006), An ancient carbon mystery, *Science*, *314*(5805), 1556–1557, doi:10.1126/science.1136110.

Panchuk, K., A. Ridgwell, and L. R. Kump (2008), Sedimentary response to Paleocene-Eocene Thermal Maximum carbon release: A model-data comparison, *Geology*, *36*(4), 315–318, doi:10.1130/G24474A.1.

Popp, M., H. Schmidt, and J. Marotzke (2016), Transition to a moist greenhouse with CO_2 and solar forcing, *Nat. Commun.*, *7*, 10,627, doi:10.1038/ncomms10627.

Schmittner, A., N. M. Urban, J. D. Shakun, N. M. Mahowald, P. U. Clark, P. J. Bartlein, A. C. Mix, and A. Rosell-Melé (2011), Climate sensitivity estimated from temperature reconstructions of the Last Glacial Maximum, *Science*, *334*(6061), 1385–1388, doi:10.1126/science.1203513.

Schneider von Deimling, T., A. Ganopolski, H. Held, and S. Rahmstorf (2006), How cold was the Last Glacial Maximum?, *Geophys. Res. Lett.*, *33*, L14709, doi:10.1029/2006GL026484.

Schubert, B. A., and A. H. Jahren (2013), Reconciliation of marine and terrestrial carbon isotope excursions based on changing atmospheric CO_2 levels, *Nat. Commun.*, *4*, 1653–1656, doi:10.1038/ncomms2659.

Shaffer, G., S. M. Olsen, and J. O. P. Pedersen (2008), Presentation, calibration and validation of the low-order, DCESS Earth System Model (Version 1), *Geosci. Model Dev.*, *1*(1), 17–51, doi:10.5194/gmd-1-17-2008.

Sherwood, S. C., S. Bony, and J.-L. Dufresne (2014), Spread in model climate sensitivity traced to atmospheric convective mixing, *Nature*, *505*(7481), 37–42, doi:10.1038/nature12829.

Svensen, H., S. Planke, A. Malthe-Sørenssen, B. Jamtveit, R. Myldebust, T. R. Ewem, and S. S. Rey (2004), Release of methane from a volcanic basin as a mechanism for initial Eocene global warming, *Nature*, *429*(6991), 542–545, doi:10.1038/nature02566.

Zachos, J. C., et al. (2005), Rapid acidification of the ocean during the Paleocene-Eocene Thermal Maximum, *Science*, *308*(5728), 1611–1615, doi:10.1126/science.1109004.

Zachos, J. C., G. R. Dickens, and R. E. Zeebe (2008), An early Cenozoic perspective on greenhouse warming and carbon-cycle dynamics, *Nature*, *451*(7176), 279–283, doi:10.1038/nature06588.

Zeebe, R. E., J. C. Zachos, and G. R. Dickens (2009), Carbon dioxide forcing alone insufficient to explain Palaeocene–Eocene Thermal Maximum warming, *Nat. Geosci.*, *2*(8), 1–5, doi:10.1038/ngeo578.